iScience

Article

Distinctly structured social behavior across three rodent strains is associated with different neural activity patterns

Graphical abstract

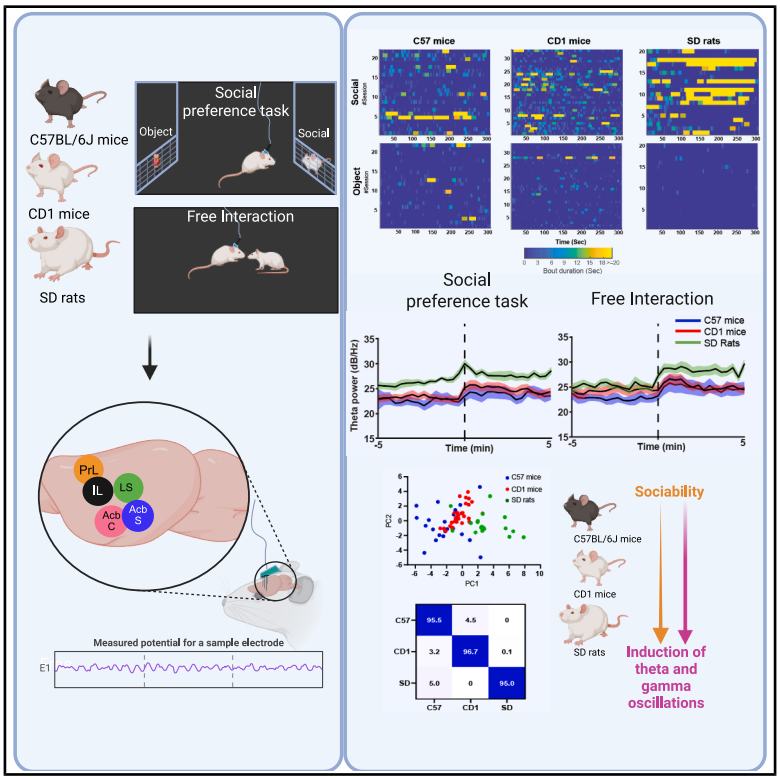

Highlights

- C57BL mice, CD1 mice, and SD rats exhibit distinct profiles of social behavior
- LFP theta and gamma oscillations in fronto-limbic areas show strain-specific differences
- C57BL mice and SD rats show opposite patterns of social behavior and LFP coherence dynamics
- Prelimbic cortex-nucleus accumbens shell coherence dominates strain-specific differences

Authors

Rishika Tiwari, Alok Nath Mohapatra, Claudio J. Mendes, Jr., Renad Jabarin, Shai Netser, Shlomo Wagner

Correspondence

rishikatiwari1998@gmail.com

In brief

Neuroscience; Behavioral neuroscience; Systems neuroscience

Tiwari et al., 2026, iScience *29*, 116119
August 21, 2026
https://doi.org/10.1016/j.isci.2026.116119

CellPress

iScience

CellPress
OPEN ACCESS

Article

Distinctly structured social behavior across three rodent strains is associated with different neural activity patterns

Rishika Tiwari,[1,5,*] Alok Nath Mohapatra,[2,3,4] Claudio J. Mendes, Jr.,[1] Renad Jabarin,[1] Shai Netser,[1] and Shlomo Wagner[1]
[1]Sagol Department of Neurobiology, Faculty of Natural Sciences, University of Haifa, Haifa, Israel
[2]Department of Psychiatry, Massachusetts General Hospital, Harvard Medical School, Boston, MA, USA
[3]Harvard Stem Cell Institute, Cambridge, MA, USA
[4]BROAD Institute of MIT and Harvard, Cambridge, MA, USA
[5]Lead contact
*Correspondence: rishikatiwari1998@gmail.com
https://doi.org/10.1016/j.isci.2026.116119

SUMMARY

Social behavior varies considerably across mammalian species, yet the neural basis for these variations remains unclear. We compared the behavior of three commonly used laboratory rodent strains (C57BL/6J and CD1 mice and SD rats) in social preference and free interaction tasks. Animals carried chronically implanted electrodes in brain regions associated with social motivation. The three strains exhibited distinctly structured social behavior: SD rats showed the strongest social motivation, CD1 mice were most active, and C57BL/6J mice displayed the most restrained behavior. Electrophysiology revealed strain- and task-specific theta and gamma power and coherence. Strikingly, SD rats displayed low baseline coherence followed by robust induction during interactions, while C57BL/6J mice exhibited opposite tendencies. Machine learning models allowed accurate strain separation based solely on brain electrophysiology, with theta and gamma coherence between the prelimbic cortex and nucleus accumbens shell playing a key role in defining distinct neuronal signatures of strain-specific social strategies.

INTRODUCTION

Social behavior is fundamental to the survival and reproductive success of most mammalian species, including rodents and humans.[1] Understanding the neural mechanisms underlying social interactions is crucial for elucidating the pathophysiology of neuropsychiatric disorders characterized by social deficits, such as autism spectrum disorder.[2,3] Laboratory rodent models allow invasive recording and manipulation of brain neuronal activity during social interaction and thus offer valuable insights into the neural substrates and mechanisms of social behavior.[4,5] Nevertheless, several distinct rodent models, including C57BL/6J (C57) mice, CD1 mice, and Sprague Dawley (SD) rats, are widely used for exploring neuronal mechanisms of social behavior, but the extent to which the studies across different models can be generalized is not determined yet. In many cases, researchers assume that brain mechanisms found in one rodent model would be similar across all models, despite behavioral distinctions between them. Previous studies have shown that SD rats exhibit higher social motivation and more consistent engagement in social interactions than C57 mice.[6] Recent evidence also suggests that CD1 mice seek social interaction more robustly than the C57 mice.[7] Here, we aimed to directly examine whether brain circuits subserving social motivation act differently in these three rodent laboratory strains.

Social behavior is orchestrated by a complex network of interconnected brain regions, with the medial prefrontal cortex (mPFC) and nucleus accumbens (Acb) playing significant roles. The mPFC is integral to social decision-making,[8] social cognition,[9] and evaluating social rewards,[10] while the Acb, as a core component of the mesolimbic dopamine system, processes social motivation and reward seeking.[3,11–13] Notably, strain-specific behavioral differences in social motivation were previously linked to distinctions in neural activity within the medial amygdala and Acb during social interactions.[6] Additionally, the lateral septum (LS), due to its anatomical connectivity, serves as a convergence point for cortical information from areas like the mPFC and hippocampus,[14] as well as limbic inputs from the amygdala, ventral tegmental area, bed nucleus of stria terminalis, and hypothalamic nuclei. This integration of cognitive, experiential, and internal state information enables the septum to coordinate appropriate behavioral outputs through its projections to downstream hypothalamic and midbrain regions. Cross-species investigations in songbirds,[15] primates,[16] rodents,[17] and humans[18] have established the LS as a key regulator of social behavior.

Local field potential (LFP) recordings offer a powerful tool to explore the dynamics of population neural activity across multiple brain regions, by capturing synchronized neuronal activity across different frequency bands, such as theta (4–12 Hz) and

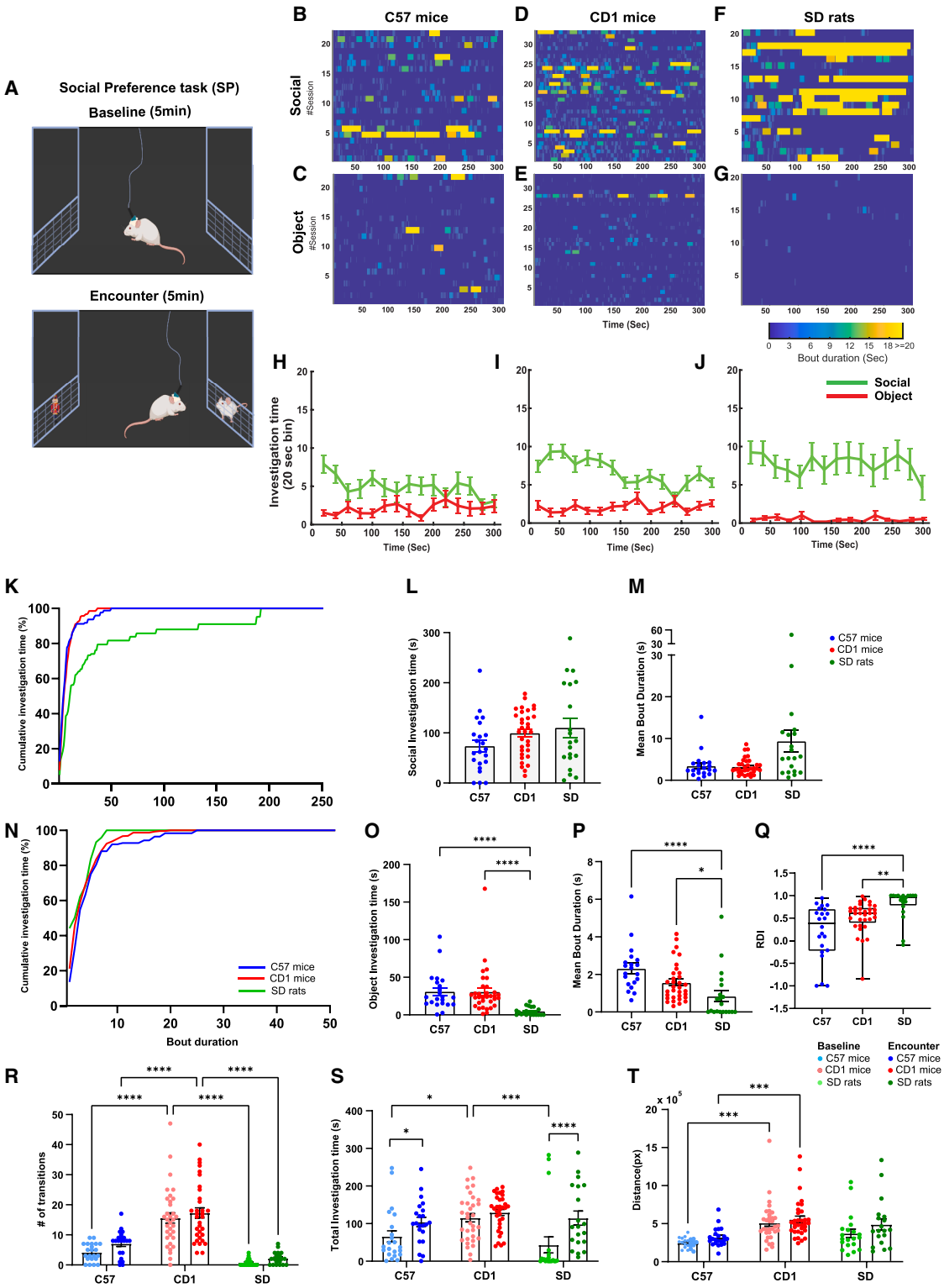

Figure 1. The three strains exhibit significant behavioral differences while performing the SP task

(A) Schematic of the social preference (SP) paradigm.

(B and C) Heatmaps of investigation bouts of C57 mice toward social (B) and object (C) stimuli during the SP task.

(D and E) As in (B) and (C) for CD1 mice.

(F and G) As in (B) and (C) for SD rats.

(legend continued on next page)

gamma (30–80 Hz) oscillations.[19] Theta oscillations are implicated in various cognitive processes, including navigation[20] and memory,[21] and often facilitate coordination across distributed brain networks.[22,23] Gamma oscillations, associated with sensory processing[24] and attentional mechanisms,[25,26] reflect local circuit synchrony.[27,28] Theta and gamma oscillations in mouse brain areas associated with social behavior were shown to reflect social memory and emotion recognition.[29,30]

The present study aims to elucidate the neural correlates associated with strain-specific differences in social behavior and motivation among C57 mice, CD1 mice, and SD rats. Utilizing chronically implanted multi-electrode arrays, we compared LFP signals simultaneously recorded in a specific set of brain regions, including areas of the mPFC, Acb, and LS, during two types of social interactions: the social preference (SP) and free interaction (FI) tasks. We hypothesized that differences in social motivation and behavior among the strains would be reflected by distinct patterns of theta and gamma rhythmicity across the various brain regions.

RESULTS

The three rodent strains show distinctly structured behavior while performing the same tasks

For comparing between C57 (n = 22 for SP, n = 23 for FI), CD1 (n = 33 for SP, n = 34 for FI), and SD (n = 20 for SP, n = 12 for FI), we used two distinct social behavior tasks. In the SP task (Figure 1A), subject animals first experienced a 5-min baseline stage with two empty chambers located at randomly chosen opposite corners of the arena. This was followed by a 5-min encounter stage, with one of the chambers now containing a social stimulus (an age- and sex-matched conspecific), while the other one containing an object (a Lego toy). In the FI task (Figure 1B), a 5-min baseline stage in an empty arena was followed by a 5-min encounter stage, after a social stimulus was introduced to the arena. It should be noted that, while in the SP task social interactions between the subject and stimulus animals were restricted by a metal mesh located at the bottom of the stimulus chamber, in the FI task social interactions were unrestricted. All animals were electrophysiologically recorded across both stages of each task, using electrode arrays chronically implanted in their brains (see details in the following text) as previously described.[31]

We used our previously described TrackRodent software[32] to analyze in detail the stimulus investigation behavior of the subject animals during the SP task. Figures 1B–1G show heatmaps of the investigation events conducted by the subjects toward each of the stimuli, color-coded according to the duration of each investigation event (henceforth termed investigation bout), separately for each strain. As apparent, while all strains displayed a clear preference to investigate the social stimulus over the object across the entire encounter (Figures 1H–1J), they exhibited striking structural variations in their investigation behavior. Specifically, SD rats exhibited very long social investigation bouts, some of which could last for more than half of the session time, while both mouse strains displayed a large number of relatively short social investigation bouts. These differences are clearly reflected by the significantly different cumulative histograms of social investigation bouts calculated for the three strains (Figure 1K). Accordingly, while no significant difference was found between the strains in the overall time the subjects investigated the social stimulus (Figure 1L), SD rats tend to show a longer mean duration of social investigation bouts, as compared to both strains of mice (Figure 1M). As for the object, while we found no difference between the two mouse strains in the various features of object investigation (Figures 1N–1P), SD rats showed lower levels of object investigation time (Figure 1O) and mean bout duration (Figure 1P). Accordingly, rats showed a higher relative discrimination index (RDI) than both mouse strains (Figure 1Q), reflecting their higher preference to investigate the social stimulus over the object.[6] Altogether, these results suggest that the structure of investigation behavior during the SP task is strain specific and mainly differ between SD rats and the two mouse strains.

Strain-specific behavioral patterns are also apparent from the number of transitions made by the subjects between stimuli, which was significantly higher in CD1 mice than in both other strains, in both stages of the session (Figure 1R). Interestingly, the total investigation time of both chambers was similar between the baseline and encounter stages only for CD1 mice,

(H–J) Mean (±SEM) investigation time (20-s time bins) toward the social (green trace) and object (red trace) stimuli along the SP session's time course for C57 mice (H), CD1 mice (I), and SD rats (J).
(K) Cumulative histograms of social investigation time (KS test, C57 vs. CD1, D = 0.95, $p < 0.0001$; C57 vs. SD, D = 0.56, $p < 0.0001$, CD1 vs. SD, D = 0.57, $p < 0.0001$).
(L) Mean (±SEM) social investigation time across different strains.
(M) Mean (±SEM) social investigation bout duration (Kruskal-Wallis test, H = 7.182, $p = 0.0279$; Dunn's MC test, CD1 vs. SD, $p = 0.058$, C57 vs. SD, $p = 0.050$).
(N) As in (L), for object investigation (KS test, C57 vs. CD1, D = 0.04, $p = 0.97$; C57 vs. SD, D = 0.98, $p < 0.0001$, CD1 vs. SD, D = 0.98, $p < 0.0001$).
(O) As in (M), for object investigation.
(P) As in (N), for object investigation (Kruskal-Wallis test, H = 32.54, $p < 0.0001$; Dunn's MC test, CD1 vs. SD, $p < 0.0001$, C57 vs. SD, $p < 0.0001$).
(Q) Mean (±SEM) RDI values across strains (Kruskal-Wallis test, H = 23.13, $p < 0.0001$; Dunn's multiple comparisons test, CD1 vs. SD, $p < 0.01$, C57 vs. SD, $p < 0.0001$).
(R) Mean (±SEM) number of transitions between the two chambers during baseline and encounter periods across strains (two-way RM ANOVA, main effect of strain, $F(2,72) = 42.09$, $p < 0.0001$, time, $F(1,72) = 7.902$, $p < 0.01$; Sidak's MC test, baseline, CD1 vs. SD, $p < 0.0001$, C57 vs. CD1, $p < 0.0001$; encounter, CD1 vs. SD, $p < 0.0001$, C57 vs. CD1, $p < 0.0001$).
(S) Mean (±SEM) total investigation time (of both stimuli) during baseline and encounter periods across strains (two-way RM ANOVA, main effect of strain, $F(2,72) = 4.158$, $p < 0.05$, time, $F(1,72) = 28.81$, $p < 0.05$, encounter, $F(2,72) = 4.820$, $p < 0.05$; Sidak's MC test, baseline, CD1 vs. SD, $p < 0.0001$, C57 vs. CD1, $p < 0.05$; baseline vs. encounter, C57, $p < 0.05$, SD, $p < 0.0001$).
(T) Mean (±SEM) distances traveled during baseline and encounter stages (two-way RM ANOVA, main effect of strains, $F(2,72) = 9.875$, $p < 0.001$, time, $F(1,72) = 9.296$, $p < 0.01$; Sidak's MC test, baseline, C57 vs. CD1, $p < 0.001$, encounter, C57 vs. CD1, $p < 0.001$). *$p < 0.05$, **$p < 0.01$, ***$p < 0.001$, ****$p < 0.0001$.

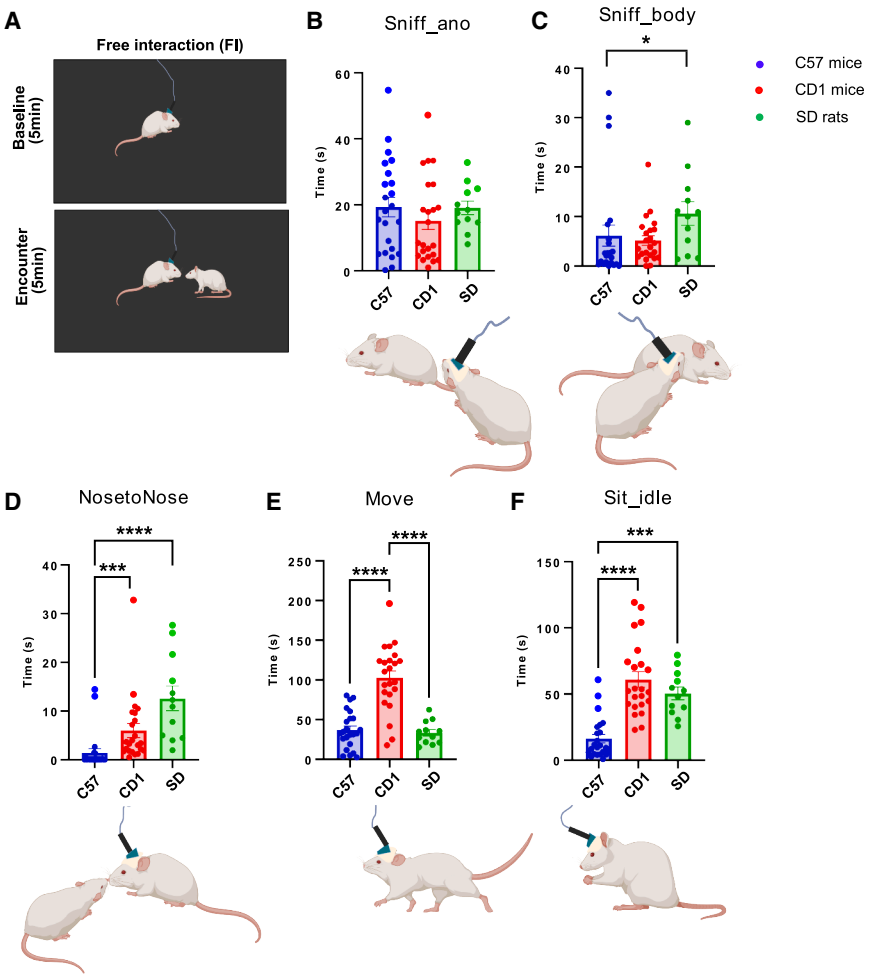

Figure 2. The three strains exhibit significant behavioral differences during free social interaction

(A) The free interaction (FI) paradigm.

(B) Mean (±SEM) anogenital sniffing time across strains.

(C) Mean (±SEM) body sniffing time across strains (Kruskal-Wallis test, H = 7.098, $p < 0.05$, Dunn's multiple comparisons test, C57 vs. SD, $p < 0.05$).

(D) Mean (±SEM) nose-to-nose interaction time across strains (Kruskal-Wallis test, H = 30.96, $p < 0.0001$, Dunn's multiple comparisons test, C57 vs. SD, $p < 0.0001$, C57 vs. CD1, $p < 0.001$).

(E and F) Comparison of non-social behaviors, such as movement (E; one-way ANOVA, F = 33.09, $p < 0.0001$, Dunn's multiple comparisons test, C57 vs. SD, $p < 0.0001$, CD1 vs. SD, $p < 0.0001$), and sitting idle (F; Kruskal-Wallis test, H = 31.14, $p < 0.0001$, Dunn's multiple comparisons test, C57 vs. SD, $p < 0.001$, C57 vs. CD1, $p < 0.0001$) across strains. $^{*}p < 0.05$, $^{***}p < 0.001$, $^{****}p < 0.0001$.

while both other strains investigated the empty chambers during baseline for less time than the stimulus-containing chambers during the interaction (Figure 1S). Finally, while we found no significant difference between the two stages in the distance traveled by the subject animals during that stage for any of the strains, CD1 mice exhibited a higher traveled distance than C57 mice in both stages (Figure 1T). Overall, these results reveal significant behavioral differences between the three strains during the SP task, with SD rats showing a higher level of SP, while CD1 mice showing a higher level of activity, especially during baseline, compared to both other strains.

For analyzing the behavior of the three strains during the FI task, we used DeepLabCut (DLC, Figures S1A–S1D)[33] for tracking both animals in the arena and used SimBA behavioral segmentation analysis[34] for quantifying the time each subject spent in one of five distinct behaviors (Figures 2B–2F). We found no difference between the strains in the time dedicated to sniffing the anogenital regions of the conspecific (Figure 2B). However, rats spent significantly more time in sniffing the body of the social stimulus, compared to C57 mice, and showed a trend toward spending more time than CD1 mice (Figure 2C). Moreover, there were significant differences between the strains in nose-to-nose interactions, with SD rats showing the highest level, CD1 mice showing a slightly lower level, and C57 mice showing the lowest level (Figure 2D). Finally, CD1 mice spent significantly more time in movement than both other strains (Figure 2E), while C57 mice showed a significantly lower level of sit-idle behavior than the other two strains (Figure 2F).

Thus, the behavior of the three strains in the FI task shows similar differences to those exhibited by them in the SP task; SD rats showed the highest level of motivation for social interaction, as reflected by their prolonged social investigation bouts and higher RDI values in the SP task and a higher level of body sniffing and nose-to-nose interactions in the FI task. In contrast, CD1 mice were the most active among the three strains, as reflected by their higher movement level during both tasks, as well as higher level of total investigation and transitions between stimuli during the SP task.

Strain-specific differences in LFP power recorded in a subset of brain areas during both tasks

We next analyzed the LFP signals recorded during the same experiments (both SP and FI sessions) from five brain regions previously linked to social behavior and motivation: the infralimbic (IL) and prelimbic (PRL) areas of the mPFC, the nucleus accumbens core (AcbC) and shell (AcbS) areas, and the LS (Figures 3A and 3B; see Table S2 for the details). Power spectral density (PSD) profiles calculated separately for each region at each stage of the various sessions demonstrated distinct power profiles for the baseline and encounter stages (Figures 3B and 3C). We then calculated the LFP power along the time course of the session for the theta (4–12 Hz) and gamma (30–80 Hz) bands, separately for each brain region. As previously reported by us,[29,35,36] in most brain regions, the social encounter was

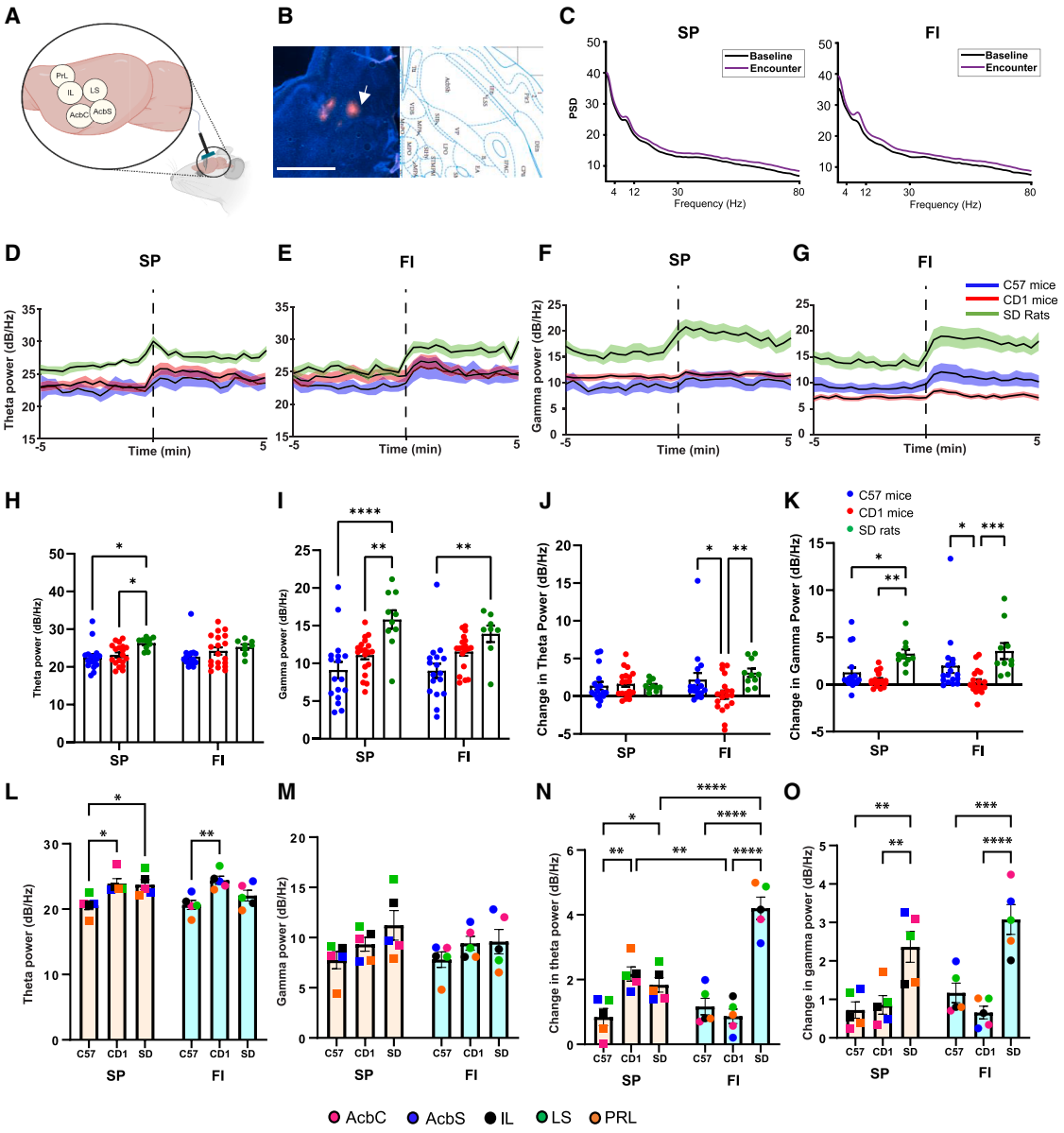

Figure 3. The three strains exhibit significant differences in brain theta and gamma power during the two tasks

(A) Schematic of the target areas and electrode probe.

(B) Example picture of electrode tip tracings in AcbS (left) and brain atlas scheme of the corresponding regions (right). Horizontal section, scale bars: 1 mm.

(C) Example PSD traces in AcbS of a single SD rat during baseline (black) and encounter (purple) during stages of SP (left) and FI (right) tasks.

(D) Trace of mean (±SEM) theta power recorded from AcbS along the baseline (−5 to 0 min) and encounter (0–5 min) during SP across all strains.

(E) Same as (D), for FI.

(F and G) As in (D) and (E), for gamma power.

(H and I) Mean (±SEM) theta (H) and gamma (I) power recorded in AcbS during baseline stage in SP (left bars) and FI (right bars) tasks across the various strains (theta power, two-way ANOVA, strain: $F(2,86) = 4.324$, $p < 0.05$; Sidak's MC test, SP: C57 vs. SD, $p < 0.05$, CD1 vs. SD, $p < 0.05$; gamma power, two-way ANOVA, strain: $F(2,86) = 14.59$, $p < 0.0001$; Sidak's MC test, SP, C57 vs. SD, $p < 0.0001$, CD1 vs. SD, $p < 0.01$, FI: C57 vs. SD, $p < 0.05$).

(J and K) Mean (±SEM) change (from baseline level) in theta (J) and gamma (K) power recorded in AcbS during the encounter stage in SP (left bars) and FI (right bars) tasks across the various strains (theta power, two-way ANOVA, interaction: $F(2,86) = 3.357$, $p < 0.05$; Sidak's MC test, FI, CD1 vs. SD, $p < 0.05$, C57 vs. CD1, $p < 0.05$; gamma power, two-way ANOVA, strain: $F(2,86) = 17.02$, $p < 0.0001$; Sidak's MC test, SP, C57 vs. SD, $p < 0.05$, CD1 vs. SD, $p < 0.01$; FI, C57 vs. CD1, $p < 0.05$, C57 vs. SD, $p < 0.05$, CD1 vs. SD, $p < 0.0001$).

(L and M) Mean (±SEM) in theta (L) and gamma (M) power in all five recorded brain regions during baseline across strains (theta power, two-way ANOVA, interaction: $F(2,24) = 12.32$, $p < 0.001$; Sidak's MC test, baseline, C57 vs. CD1, $p < 0.05$; FI, C57 vs. CD1, $p < 0.01$; gamma power, two-way ANOVA, strain: $F(2,24) = 3.526$, $p < 0.05$).

(legend continued on next page)

accompanied by an elevation in the LFP power relative to baseline, in both theta (Figure S2) and gamma (Figure S3) bands. Nevertheless, strain-specific differences were found in both the baseline power level and the level of power change during encounter (Δpower), and these differences were task dependent. For example, in the AcbS (Figures 3D–3G), we found a higher level of both theta and gamma power during SP baseline in SD rats, compared to both mouse strains, while during FI baseline, only the difference between SD rats and C57 mice in gamma power was statistically significant (Figures 3H and 3I). In contrast, during the encounter stage, we found more strain-specific differences in the FI task, with both SD rats and C57 mice showing significantly stronger power change than CD1 mice in both the theta and gamma bands (Figures 3J and 3K), while during SP encounter, SD rats exhibited a higher level of power change than the two mouse strains, but only in the gamma range. Thus, the differences in LFP power between the strains were task-, band-, and brain region specific. It should be noted, however, that in almost all brain regions SD rats showed a significantly higher level (compared to both mouse strains) of change in both theta and gamma power during FI encounter (Figures S2 and S3).

We then compared the mean power across all brain regions between the three strains, as a measure of the general change in theta and gamma rhythmicity in this network. We found that C57 mice showed significantly a lower level of theta power compared to both other strains during the SP baseline and to CD1 mice during the FI baseline (Figure 3L). No significant difference at baseline was found for gamma power (Figure 3M). During the FI encounter stage, rats showed a significantly higher level of change in both theta and gamma power, as compared to the other strains. The same difference was found for the gamma change in SP sessions, while for theta power change C57 mice showed a lower level than both SD rats and CD1 mice (Figures 3N–3O). Notably, when intra-species differences between the tasks were examined, SD rats exhibited a higher power change during FI sessions compared to SP sessions in both theta and gamma bands, while CD1 mice showed a higher level of theta power change during SP sessions, as compared to FI sessions. Assuming that a higher level of theta power change across all brain regions is associated with a higher level of a certain internal state,[30] these results suggest that SD rats exhibit a stronger internal state during the encounter stage of FI sessions, compared to SP sessions, while CD1 mice show the opposite tendency.

Strain-specific LFP coherence differences during both baseline and social interaction

While strain-dependent variations in LFP power may be attributed to differences in cell size or number, the correlation in neural activity between distinct brain regions is not expected to be influenced by these types of factors but rather by the level of inter-regional communication. Such correlation between brain regions is reflected by LFP coherence, widely known to be modulated when brain regions are involved in processing the same cognitive task.[37,38] We previously demonstrated significant coherence modulation between various remote brain regions during social interaction for each one of the three strains.[29,30,36] We therefore examined the coherence across the 5-brain region network examined by us in this study, for all three strains. Notably, this was done only for brain region pairs for which we had enough recordings ($n \geq 5$) from all strains (Figure 4A). Interestingly, we observed robust strain-dependent differences in both theta and gamma coherence already during baseline, before the introduction of stimuli to the arena. As apparent in Figures 4B and 4C, C57 mice showed a significantly higher level of both theta and gamma coherence during both SP and FI sessions, as compared to both SD rats and CD1 mice (only the difference from CD1 mice in gamma coherence during FI baseline did not reach statistical significance). These results strongly suggest a robust internal state exhibited specifically by C57 mice already at the baseline stage.

When analyzing the mean change in coherence taking place across the 5-brain region network during the encounter, we also observed robust differences between the various strains (Figures 4D and 4E), but these differences were opposite to those observed during baseline. Mainly, SD rats always showed an increase in coherence, and this change was significantly different from the change exhibited by C57 mice, which tended to display a small decrease in coherence. CD1 mice showed a tendency toward no change in coherence, except for theta coherence during the SP encounter, which increased and was significantly different from that in C57 mice but not from that in SD rats. This result, which is similar to the change in theta power during the SP encounter exhibited by CD1 mice (Figure 3N), suggests an internal state of CD1 mice, induced specifically during the SP encounter.

Overall activity in the network strongly distinguishes between the three strains

To further examine how much the overall pattern of electrophysiological activity in the 5-brain region network differs between the stages and strains, we used principal-component analysis (PCA) to cluster the various strains and stages according to all electrophysiological measures (see Table S2 for a list of all measures), separately for SP and FI sessions (Figures 5A–5H). We found that in all strains the baseline and encounter stages showed separable clustering, suggesting substantial electrophysiological differences between them. However, the mean distance between the baseline and encounter clusters was lowest for CD1 mice, which may reflect the fact that this strain did not show any clear change in activity (traveled distance, transitions, and total investigation) between the two stages of the SP task, in contrast to the other strains (Figures 1S–1U). Interestingly, the distance

(N and O) Mean (±SEM) change in theta (N) and gamma (O) power in all five recorded brain regions during encounter across strains (theta power, two-way ANOVA, interaction: $F(2,24) = 25.35$, $p < 0.0001$, strain: $F(2,24) = 32.80$, $p < 0.0001$, task: $F(1,24) = 4.796$, $p < 0.05$; Sidak's MC test, SP, C57 vs. CD1, $p < 0.01$, C57 vs. SD, $p < 0.05$; FI, C57 vs. SD, $p < 0.0001$, CD1 vs. SD, $p < 0.0001$; SP vs. FI, CD1, $p < 0.01$, SD, $p < 0.0001$; gamma power, two-way ANOVA, strain: $F(2,24) = 27.93$, $p < 0.0001$; SP, CD1 vs. SD, $p < 0.01$, C57 vs. SD, $p < 0.01$; FI, C57 vs. SD, $p < 0.001$, CD1 vs. SD, $p < 0.0001$). Each data point represents the change in power in one brain region averaged over all the recorded sessions (see color code below). *$p < 0.05$, **$p < 0.01$, ***$p < 0.001$, ****$p < 0.0001$.

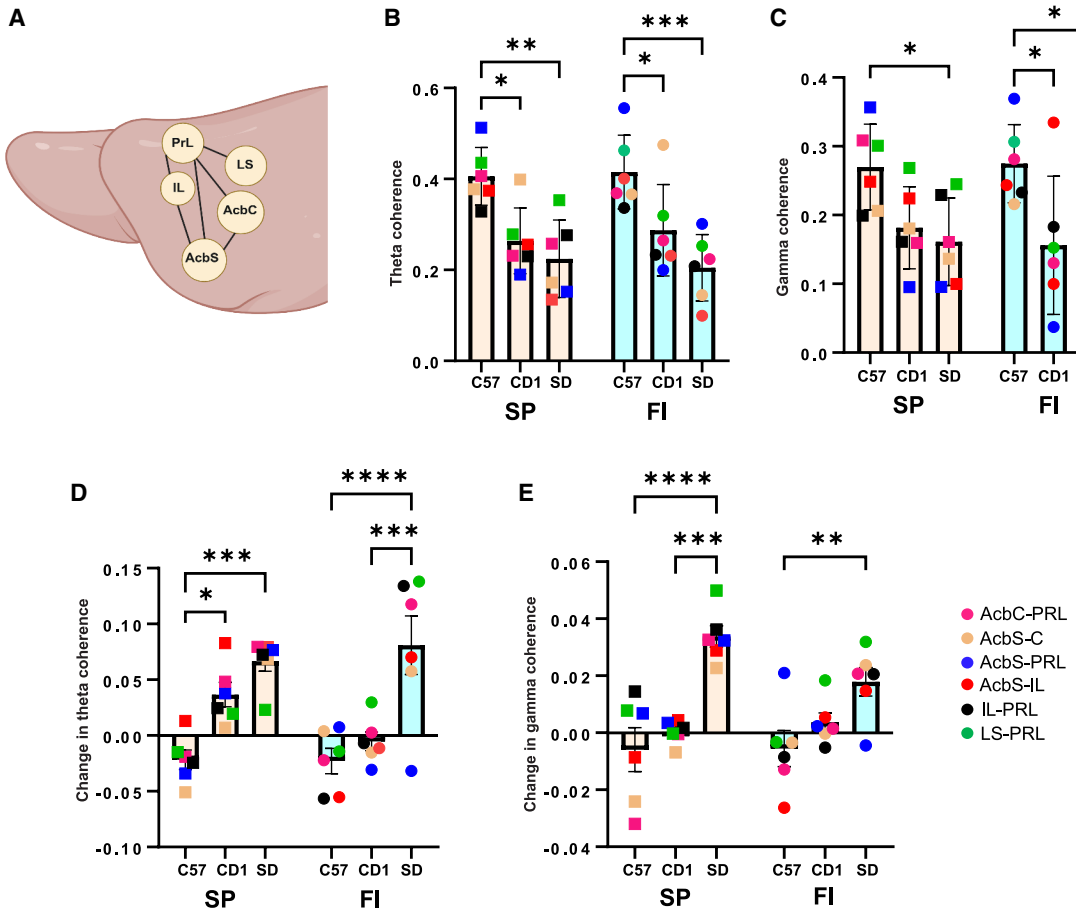

Figure 4. LFP theta and gamma coherence in the network of brain regions was higher in C57 mice during baseline and in SD rats during social interaction

(A) Schematic of the brain region pairs used for coherence calculation.

(B and C) Mean (±SEM) theta (B) and gamma (C) coherence among the six pairs of brain regions, as recorded during the baseline stage of the SP (left bars) and FI (right bars) tasks across the various strains (theta coherence, two-way ANOVA, strain: $F(2,30) = 18.77$, $p < 0.0001$; Sidak's MC test, SP: C57 vs. SD, $p < 0.01$, C57 vs. CD1, $p < 0.05$, FI: C57 vs. CD1, $p < 0.05$, C57 vs. SD, $p < 0.001$; gamma coherence, two-way ANOVA, strain: $F(2,30) = 9.736$, $p < 0.001$ Sidak's MC test, SP: C57 vs. SD, $p < 0.05$, FI: C57 vs. CD1, $p < 0.05$, C57 vs. SD, $p < 0.05$).

(D and E) Mean (±SEM) change (from baseline level) in theta (D) and gamma (E) coherence among the six pairs of brain regions, as recorded during the encounter stage of the SP (left bars) and FI (right bars) tasks, across the various strains (theta coherence, two-way ANOVA, strain: $F(2,24) = 24.06$, $p < 0.0001$; Sidak's MC test, SP: C57 vs. SD, $p < 0.001$, C57 vs. CD1, $p < 0.05$, FI: C57 vs. SD, $p < 0.0001$, CD1 vs. SD, $p < 0.001$; gamma coherence, two-way ANOVA, strain: $F(2,24) = 21.39$, $p < 0.0001$; Sidak's MC test, SP: C57 vs. SD, $p < 0.0001$, CD1 vs. SD, $p < 0.001$, FI: C57 vs. SD, $p < 0.01$). Each data point represents the mean change in coherence in one pair of brain regions during all the recorded sessions (see color code to the right). $^{*}p < 0.05$, $^{**}p < 0.01$, $^{***}p < 0.001$, $^{****}p < 0.0001$.

between stages was highest for C57 mice in the SP task and for SD rats in the FI task, suggesting a task-dependent internal state differentially induced during the encounter in each of these strains. Moreover, while in the case of CD1 mice and SD rats the SP encounter stage was clustered to the right of the baseline stage along the PC1 axis, the opposite relationship between the clusters was observed for C57 mice. Since all clusters originated from the same PCA, this suggests an opposite change in network activity from SP baseline to encounter between C57 mice and the other strains. This result again suggests a unique internal state induced in C57 mice during the SP encounter stage.

When examining the clustering of the three strains separately for each stage, we observed that for both tasks, SD rats became more distant from the two mouse strains, which became less separable from each other, during the encounter stage as compared to the baseline (Figures 5I–5N). These similarities in clustering of the three strains between the tasks suggest that the distinct changes in electrophysiology between the strains observed during the task are indeed due to the social encounter experienced by the subjects in both tasks.

We then used a random forest classifier to examine if the three strains may be classified according to their brain activity and to determine which electrophysiological features are important for such classification. We found that for SP sessions, all three strains could be very well classified with >90% accuracy using the electrophysiological features recorded either during baseline (Figures 6A and 6B) or during the encounter (Figures 6C and 6D). For FI sessions we found good classification with >80%

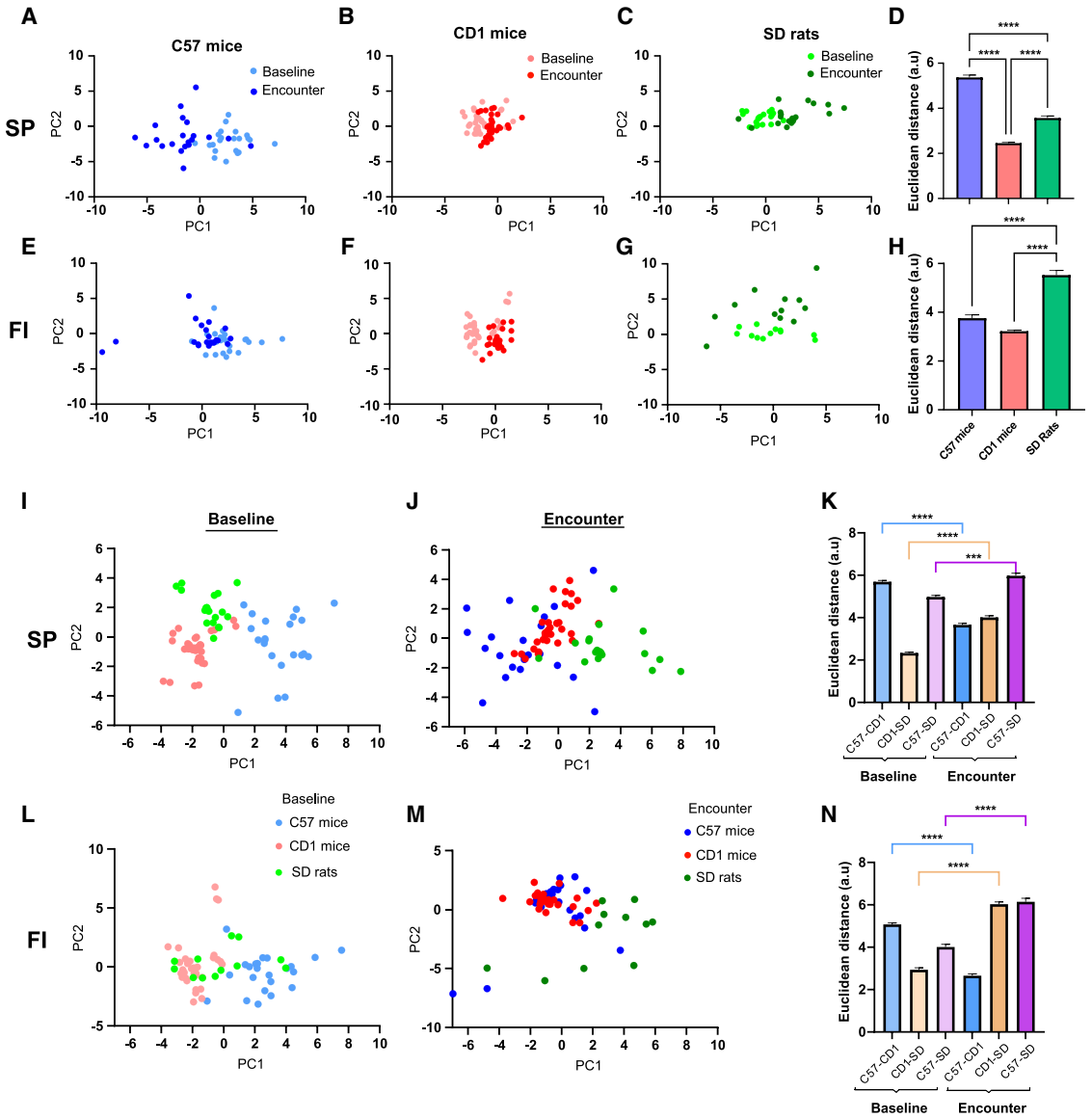

Figure 5. LFP features during social interactions result in distinct clusters for the various stages and strains

(A) 2D PCA plot based on all (22) LFP features, showing different clusters for the baseline and encounter stages of all SP sessions performed by C57 mice (explained variance of PC1 = 24.46%, PC2 = 17.21%).

(B) Same as (A), for CD1 mice.

(C) Same as (A), for SD rats.

(D) Mean (±SEM) Euclidean distance between each point in baseline and interaction period clusters across different strains.

(E–H) Same as (A)–(D), for FI sessions.

(I) 2D PCA plot based on all LFP features, showing distinct clusters for the three strains during the baseline stage of SP.

(J) Same as (I), for the encounter stage.

(K) Mean (±SEM) Euclidean distance between clusters of each pair of strains during the baseline and encounter stages of all SP sessions.

(L–N) Same as (I)–(K), for all FI sessions. ***$p < 0.001$, ****$p < 0.0001$.

accuracy during the encounter (Figures 6G and 6H). However, during the baseline stage, the accuracy for SD rats' classification was only 51.1%, while classification of the two mouse strains achieved >80% accuracy (Figures 6E and 6F). In all cases, classification using the experimental (true) data was significantly better than using shuffled data (Figure S4).

We then examined which of the 22 electrophysiological features (see Table S2) contributed significantly to the classification of the various strains, as compared to shuffled data. Interestingly, we found that both theta and gamma coherence between PRL and AcbS contributed significantly to the classification at all four stages (baseline and encounter of both tasks). Two other

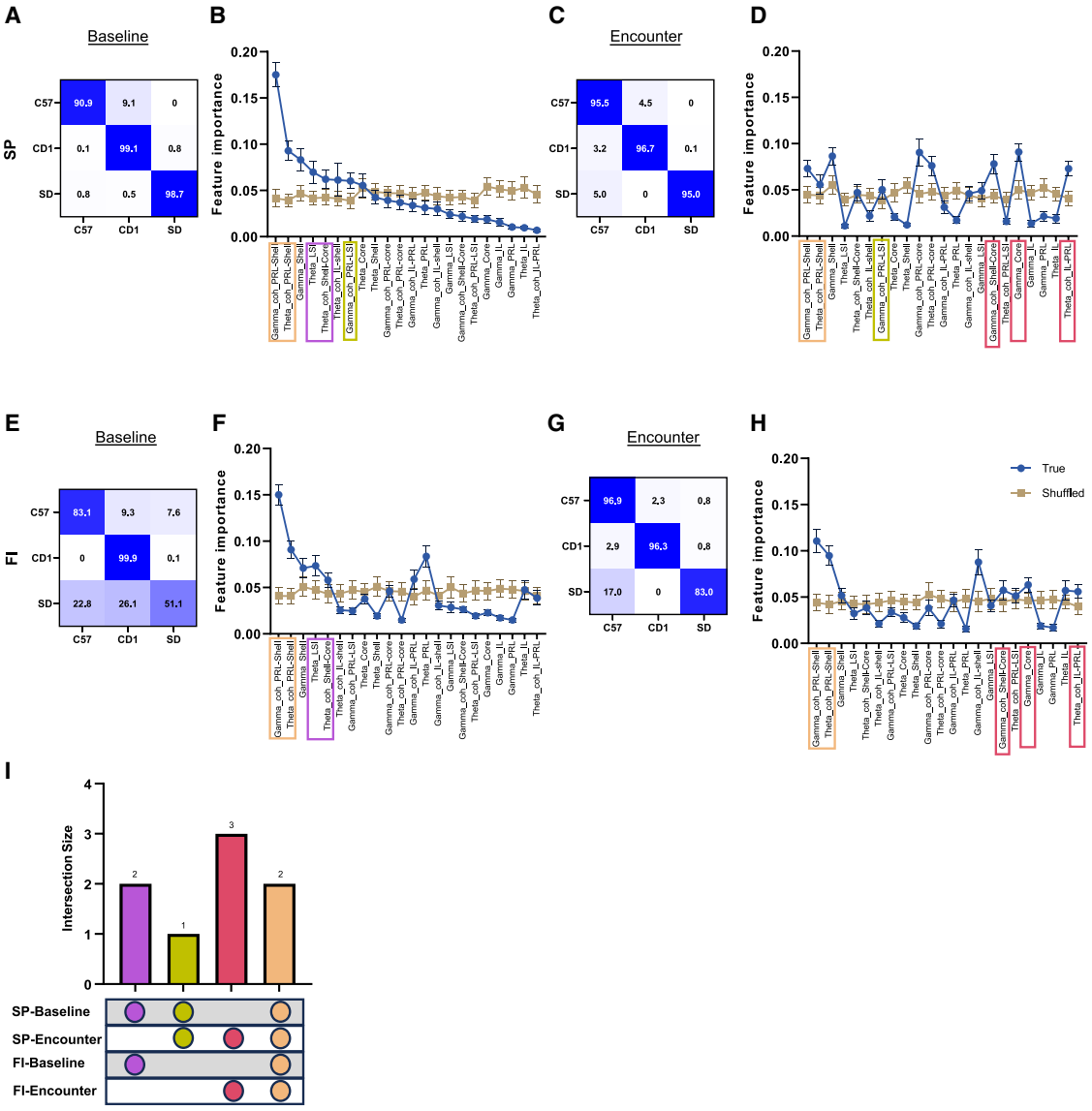

Figure 6. A random forest classifier model learns to predict the strains based on the LFP features

(A) A confusion matrix for the classifier during SP task in the baseline stage. Percentage of predicted cases is written in each block.

(B) A line plot showing importance of each feature in the classifiers trained with true labels (blue) and shuffled labels (ginger ale).

(C and D) Same as (A) and (B) for encounter stage of the SP task.

(E and F) Same as (A) and (B) for baseline stage of the FI task.

(G and H) Same as (A) and (B) for encounter stage of the FI task.

(I) An UpSet plot showing the number of shared features with higher importance in true label data than shuffled label data across all tasks and stages. The boxes on the *y* axis titles in (B), (D), (F), and (H) are color-coded as per the UpSet plot to indicate the exact features.

features (theta power in the LS and theta coherence between AcbS and AcbC) contributed significantly to the classification during the baseline stage of both tasks. Three more features (gamma power in AcbC, gamma coherence between AcbS and AcbC, and theta coherence between IL and PRL) contributed significantly to the classification during the encounter stage of both tasks and another feature (gamma coherence between PRL and LS) contributed significantly to both stages of the SP task (but not during the FI task) (Figure 6I). Thus, distinct features seem to vary between the strains in a stage- and task-dependent manner.

Activity of CamKII+ neurons in mPFC is differentially modulated during social interaction in C57 mice and SD rats

Finally, we examined if strain-dependent differences in neural activity during social interactions may be observed not only at the brain-region level but also at the level of specific neuronal

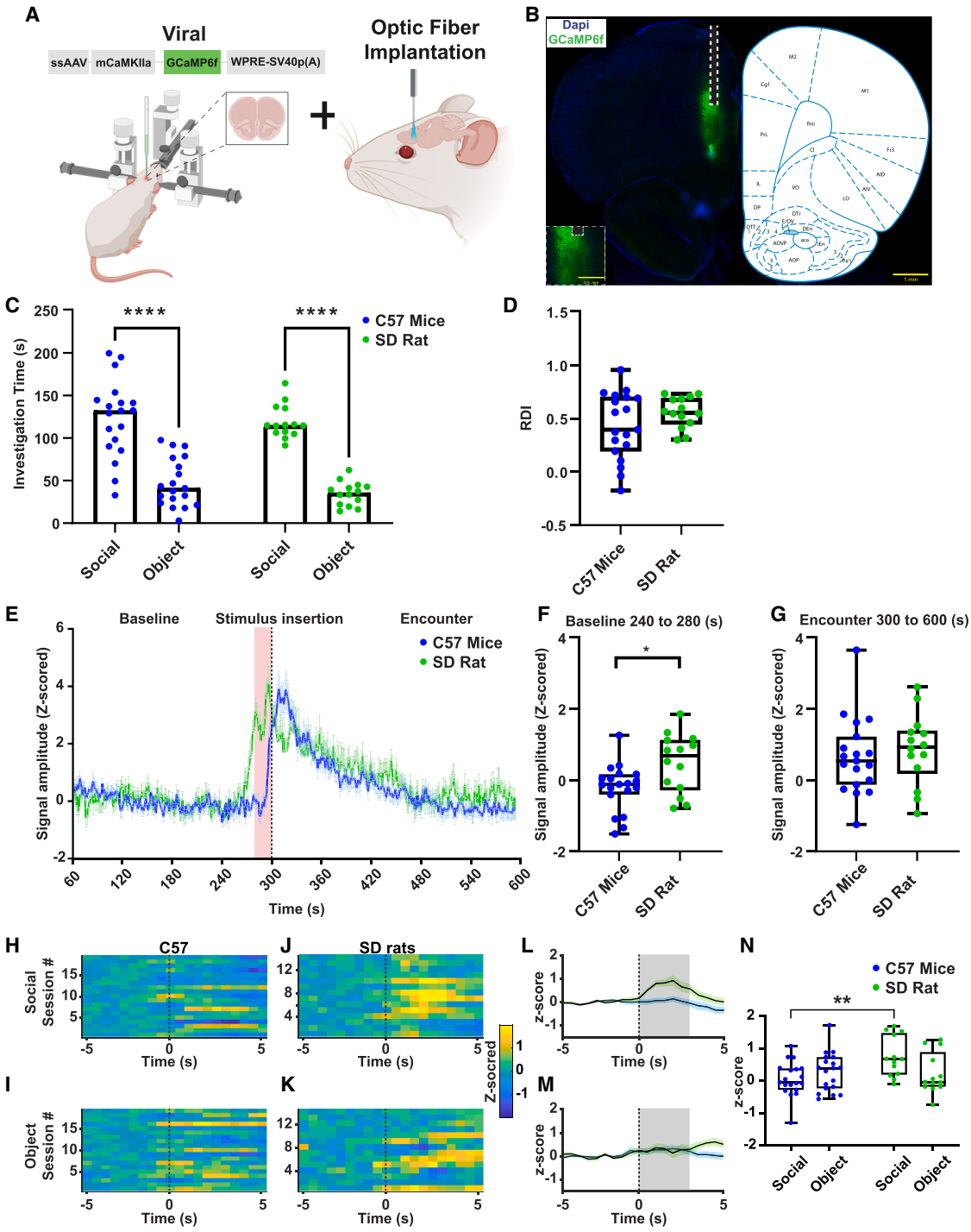

Figure 7. Distinct activity profile of PRL CamKII+ neurons during social interaction in C57 mice and SD rats

(A) A schematic of viral injection and optic fiber implantation in the PRL.

(B) A fluorescent microscopy picture of a brain slice from implanted rat, showing GCaMP6f expression and optic fiber track in the PRL alongside a brain atlas scheme of the mPFC area. Scale bars represent 1 mm in the overview image and 0.5 mm in the magnified image.

(C) Mean (±SEM) social and object investigation times for the recorded C57 mice and SD rats (two-way RM ANOVA, stimulus, $F(1,31) = 98.09$, $p < 0.0001$; social vs. object, C57 and SD, $p < 0.0001$).

(D) Mean (±SEM) RDI values for recorded animals of the two strains.

(E) A trace of raw signal (*Z* scored) along the time course of the baseline and encounter SP stages. The entire period used for stimulus insertion is marked by a red bar.

(legend continued on next page)

populations. For that, we used fiber photometry following viral vector-mediated expression of the genetic calcium indicator GCaMP6f (Figures S5A and S5B) to record calcium signals in PRL CamKII+ neurons (Figures 7A and 7B) of C57 mice (n = 14) and SD rats (n = 19) performing the SP task, where both strains showed normal SP (Figures 7C and 7D). First, we Z-scored the calcium signal recorded across the entire baseline and encounter stages and compared the mean Z-scored signals between the two strains. Similar to the LFP power (Figures S2 and S3), both strains exhibited a general pattern of a stable calcium signal during baseline, increased signal at the beginning of the encounter stage, and then a gradual decrease along the encounter stage. However, the increase in calcium signal occurred earlier in SD rats, as compared to C57 mice (Figure 7E). To make sure this earlier increase in signal does not reflect a burst of locomotion per se, we looked for a possible correlation between animal speed and calcium signal during the pre-encounter stage (first 250 s of the session) in SD rats and found no such correlation (Pearson correlation, r = 0.011, p = 0.513, n = 3,500 frames). This early elevation, which started slightly before stimulus insertion (labeled by a red bar), may therefore reflect the expectation of social interaction and was significantly stronger in SD rats than in C57 mice (Figure 7F). In contrast, the general calcium response during the encounter stage did not show a significant difference between the two strains (Figure 7G).

We further examined possible differences in calcium response between the two strains by extracting the signals around the discrete events of stimulus investigation bouts and averaging them separately for each stimulus, as previously described.[39] While no strain-dependent difference was found in the responses during object investigation, social investigation bouts elicited significantly stronger responses in SD rats than in C57 mice (Figures 7H–7N). To make sure that this difference is not due to the fact that SD rats exhibit longer social investigation bouts than C57 mice (Figure 1N), we repeated the same analysis using only investigation bouts that were longer than 6 s. When analyzing the responses across the first 5 s of these bouts, when both rats and mice were busy investigating the stimulus, we again observed no strain-dependent difference during object investigation but a significantly higher response during social investigation in SD rats, compared to C57 mice (Figures S6A–S6G). Finally, to validate that the response differences between SD rats and C57 mice are not due to movement artifacts while the animals approach the chambers, we analyzed the responses while the animals investigated the empty chamber during the baseline stage. We found a significant difference between the strains also at this stage, but in the opposite direction to the encounter stage, with C57 mice showing a stronger response than SD rats (Figure 7O). Thus, the stronger response during social investigation bouts in SD rats cannot be attributed to movement artifacts.

Altogether, these results show that even for the same neuronal population, SD rats and C57 mice show distinct responses to the social stimulus during the SP task, with earlier (compared to stimulus insertion) and stronger (during stimulus investigation) responses to social stimuli exhibited by SD rats, suggesting higher motivation for social interaction in these animals.

DISCUSSION

Here, we explored neural correlates associated with strain-specific differences in social behavior and motivation among C57 mice, CD1 mice, and SD rats. Our behavioral analysis revealed three distinct profiles of social interaction among the tested strains. SD rats demonstrated the highest level of social motivation, characterized by a tendency for prolonged social investigation bouts and higher RDI values during SP sessions and more nose-to-nose interactions during FI sessions. In contrast, both mouse strains displayed fragmented social behavior patterns, characterized by numerous short social investigation bouts rather than sustained interactions. These findings extend our previous observations[6] and reinforce the notion that SD rats exhibit more motivated and sustained social engagement, compared to the two mouse strains. Of the mouse strains, CD1 mice exhibited higher overall activity levels, including a higher number of transitions between stimuli and greater movement during both tasks. This hyperactive phenotype may reflect a distinct approach to stimulus exploration, where information gathering occurs through rapid sampling rather than sustained engagement. This may suggest a higher level of curiosity exhibited by CD1 mice. In contrast, C57 mice showed the most restrained social behavior, consistent with previous characterizations of this strain as less socially motivated.[7] These behavioral differences seem to reflect distinct innate tendencies likely stemming from evolutionarily driven genetic variations. Rats, being naturally more prosocial than mice in their ecological niches,[40] may have evolved neural circuits that favor sustained social engagement. The fragmented investigation pattern observed in mice might represent an adaptive strategy balancing social information gathering with vigilance for potential threats.

The behavioral differences described earlier were accompanied by distinct electrophysiological patterns across the network of brain regions recorded by us. SD rats consistently showed a higher baseline power level in the Acb shell, suggesting an

(F) Mean (±SEM) signal amplitude before stimulus insertion (unpaired t test, t = 2.609, $p < 0.05$, the exact period is denoted above).
(G) Mean (±SEM) signal amplitude during the encounter stage (the exact period is denoted above).
(H) A heatmap of CamKII+ neuron signals recorded 5 s before and 5 s after the beginning of social investigation bouts (1-s time bins) in C57 mice. Each line represents the mean Z-scored signal across all bouts of the same session.
(I) Same as (H), for object investigation bouts.
(J and K) Same as (H) and (I), for SD rats.
(L) Traces of mean (±SEM) calcium signal recorded during social investigation bouts in C57 mice (blue) and SD rats (green).
(M) Same as (L), for object investigation bouts.
(N) Comparison of mean (±SEM) calcium signal recorded during social and object investigation bouts between C57 mice and SD rats (two-way ANOVA, interaction, F(1,60) = 6.091, $p < 0.05$, stimulus, F(1,60) = 4.624, $p < 0.05$; social, C57 vs. SD, $p < 0.01$).

inherently more active mesolimbic reward system that may predispose them to seek rewards more vigorously. The task-dependent differences in power modulation were particularly striking. During FI sessions, SD rats exhibited the strongest increases in both theta and gamma power across the network, suggesting higher reward-driven neural activity during unrestricted social encounters, compared to the restricted social interactions allowed during the SP task. This pattern contrasts with the more modest power changes observed in mice during FI sessions, potentially reflecting their more cautious approach to unrestricted social interaction. Yet, while C57 mice showed exactly the same level of LFP power in SP and FI sessions, CD1 mice exhibited significantly higher levels of theta power and coherence during SP sessions, compared to FI sessions. The restriction of this enhanced activity to the theta band suggests that it is not due to generally higher neural activity but rather reflects a cognitive state that involves a higher level of coordinated activity in the network. We suggest that this state characterizes the uniquely high level of stimulus exploration exhibited by CD1 mice during all stages of the SP task and may reflect their curiosity to explore the content of the stimulus chambers.

Perhaps our most intriguing finding was the distinct coherence patterns observed across the brain region network between the strains. C57 mice exhibited significantly higher baseline coherence in both theta and gamma bands, compared to both other strains. This elevated baseline coherence may reflect a heightened internal state already at this stage, possibly related to the higher level of general anxiety or vigilance characteristic of this strain. Paradoxically, C57 mice showed minimal or even negative coherence changes during social encounters, contrasting sharply with the robust coherence increases observed in SD rats. This pattern suggests that, at least for this network of brain regions, C57 mice may already be operating near their maximum network coordination capacity at baseline, leaving little room for further synchronization during social encounters. SD rats, conversely, showed lower baseline coherence but robust increases during social encounters, particularly during FIs. This pattern suggests a relaxed state during baseline, which is replaced by a high motivational state in response to rewarding stimuli such as social interactions. CD1 mice, on the other hand, displayed more robust enhancement in coherence during the SP task as compared to the FI task, which may result from higher curiosity due to the presence of chambers in the SP task.

Our PCA analysis, integrating all electrophysiological features measured by us across the network, revealed that each strain employs fundamentally different patterns of neural activity when transitioning from baseline to social encounter. The finding that the C57 mice baseline and encounter clusters are located oppositely to the other strains along the PC1 axis during SP sessions suggests qualitatively different neural processes, consistent with the cautious behavior exhibited by C57 mice.

The observation that strain differences become more pronounced during the encounter stage of the FI task could suggest that the genetic variations are most apparent under unrestricted social interactions. The relatively preserved clustering of mouse strains together, distinct from rats, suggests that in this case the phylogenetic distance may be a significant factor in determining neural response patterns.

The high classification accuracy achieved by our random forest algorithm (>90% for SP, >80% for FI) demonstrates that the strain-specific neural signatures revealed by us are robust and consistent. The identification of theta and gamma coherence between PRL and AcbS as key discriminating features across all conditions highlights the importance of neural communication between these regions[41,42] in defining strain-specific behavior in general, regardless of a rewarding stimulus. The finding that theta and gamma coherence within Acb subregions and mPFC areas[43,44] contributed to strain classification specifically during the social interaction stage of both tasks suggests that these features represent synchronized local neural activity involved in social motivation in a strain-specific manner.

Our fiber photometry recordings from prelimbic CaMKII+ neurons provided crucial validation of strain differences at the cellular level. The finding that SD rats showed earlier calcium signal elevation before stimulus introduction suggests anticipation of the social interaction, which fits their high level of social motivation, in contrast to the cautious approach demonstrated by C57 mice. The stronger calcium response observed in SD rats, as compared to C57 mice, specifically during social investigation bouts also fits with the higher social motivation of SD rats and further confirms that strain differences extend to the activity levels of specific neuronal populations during social encounters.

Limitations of the study

Several limitations of our study should be considered. First, our analysis focused mainly on LFPs, which primarily reflect coordinated synaptic activity at the population level[45] rather than action potentials of single units. Future studies incorporating single-unit recordings could provide complementary insights into strain-specific differences in neural coding during social interactions. Second, our recordings reveal neural correlates of the distinct behavioral profiles exhibited by the three strains but do not demonstrate a causal connection between the various behavioral and neural patterns. Future studies using optogenetic or chemogenetic manipulations may provide such causal links. Third, our findings were obtained from adult males, and it remains to be determined whether similar strain differences exist in females or emerge during different developmental periods. Fourth, our fiber photometry recordings were limited to mPFC glutamatergic neurons. Future studies may reveal how the activity of the various GABAergic neuronal populations in this area differs between the distinct strains. Finally, whereas SD rats and CD1 mice were tested in a black arena, C57 mice were tested in a white one. While all experiments were conducted under dim red light, which does not allow the animals to see the arena's color, we cannot exclude the possibility that it may have affected their behavior.

The present study reveals profound strain-specific differences in both behavioral and electrophysiological patterns during two social behavior tasks among three commonly used laboratory rodent strains: C57 mice, CD1 mice, and SD rats. Our findings challenge the widespread assumption that neural mechanisms underlying social behavior are generally similar across common rodent models and highlight the importance of considering strain-specific characteristics when interpreting the results of social neuroscience research. Moreover, our findings emphasize

the critical importance of strain selection in social neuroscience research and suggest that the diversity of rodent models may better represent the natural variation in social behavior than previously appreciated. Rather than viewing strain differences as experimental noise, our results suggest that they should be considered valuable models of different social phenotypes and strategies, each offering unique insights into the neural mechanisms of social behavior.

The identification of strain-specific electrophysiological signatures of social behavior provides a foundation for developing more targeted approaches to understanding and treating social behavior disorders. As we move toward precision medicine approaches in neuropsychiatry, recognizing and leveraging natural variation in animal models may prove essential for developing effective interventions for the diverse presentations of social behavior difficulties in human populations.

RESOURCE AVAILABILITY

Lead contact

Further information and requests for resources should be directed to and will be fulfilled by the lead contact, Rishika Tiwari (rishikatiwari1998@gmail.com).

Materials availability

This study did not generate new, unique reagents.

Data and code availability

- All data and codes are available at Mendeley data: https://doi.org/10.17632/zpb4vhkyvg.1.
- Any additional information required to reanalyze the data reported in this manuscript will be available from the lead contact upon request.

ACKNOWLEDGMENTS

This study was supported by the Israel Science Foundation (2220/22 to S.W.), the Ministry of Health of Israel (3-19884 for PainSociOT to S.W.), the German Research Foundation (DFG) (SH 752/2-1 to S.W.), the Congressionally Directed Medical Research Programs (CDMRP) (AR210005 to S.W.), the United States-Israel Binational Science Foundation (2019186 to S.W.), and the Horizon EUROPE European Research Council (ERC-SyG oxytocINspace).

AUTHOR CONTRIBUTIONS

Conceptualization, R.T., S.N., and S.W.; data curation, R.T. and S.N.; formal analysis, C.J.M.Jr., and R.T.; funding acquisition, S.W.; investigation, A.N.M., C.J.M.Jr., R.J., and R.T.; methodology, R.T. and S.N.; project administration, S.N. and S.W.; resources, S.N.; software, S.N. and R.T.; supervision, S.N. and S.W.; validation, R.T., S.N., and S.W.; visualization, R.T., S.N., and S.W.; writing – original draft, R.T., S.N., and S.W.; writing – review and editing, A.N.M., R.T., S.N., and S.W.

DECLARATION OF INTERESTS

The authors declare no competing interests.

STAR★METHODS

Detailed methods are provided in the online version of this paper and include the following:

SUPPLEMENTAL INFORMATION

Supplemental information can be found online at https://doi.org/10.1016/j.isci.2026.116119.

Received: November 20, 2025
Revised: April 5, 2026
Accepted: May 11, 2026

REFERENCES

1. Froemke, R.C., and Young, L.J. (2021). Oxytocin, Neural Plasticity, and Social Behavior. Annu. Rev. Neurosci. *44*, 359–381. https://doi.org/10.1146/annurev-neuro-102320-102847.
2. Guo, M., and Sun, L. (2023). From rodents to humans: Rodent behavioral paradigms for social behavioral disorders. Brain Circ. *9*, 154–161. https://doi.org/10.4103/bc.bc_48_23.
3. Mohapatra, A.N., and Wagner, S. (2023). The role of the prefrontal cortex in social interactions of animal models and the implications for autism spectrum disorder. Front. Psychiatr. *14*, 1205199. https://doi.org/10.3389/fpsyt.2023.1205199.
4. Jabarin, R., Netser, S., and Wagner, S. (2022). Beyond the three-chamber test: toward a multimodal and objective assessment of social behavior in rodents. Mol. Autism *13*, 41. https://doi.org/10.1186/s13229-022-00521-6.
5. Moulin, T.C., Covill, L.E., Itskov, P.M., Williams, M.J., and Schiöth, H.B. (2021). Rodent and fly models in behavioral neuroscience: An evaluation of methodological advances, comparative research, and future perspectives. Neurosci. Biobehav. Rev. *120*, 1–12. https://doi.org/10.1016/j.neubiorev.2020.11.014.
6. Netser, S., Meyer, A., Magalnik, H., Zylbertal, A., de la Zerda, S.H., Briller, M., Bizer, A., Grinevich, V., and Wagner, S. (2020). Distinct dynamics of social motivation drive differential social behavior in laboratory rat and mouse strains. Nat. Commun. *11*, 5908. https://doi.org/10.1038/s41467-020-19569-0.
7. Ramsey, L.A., Holloman, F.M., Hope, B.T., Shaham, Y., and Venniro, M. (2022). Waving Through the Window: A Model of Volitional Social Interaction in Female Mice. Biol. Psychiatry *91*, 988–997. https://doi.org/10.1016/j.biopsych.2021.10.023.
8. Euston, D.R., Gruber, A.J., and McNaughton, B.L. (2012). The Role of Medial Prefrontal Cortex in Memory and Decision Making. Neuron *76*, 1057–1070. https://doi.org/10.1016/j.neuron.2012.12.002.
9. Bicks, L.K., Koike, H., Akbarian, S., and Morishita, H. (2015). Prefrontal Cortex and Social Cognition in Mouse and Man. Front. Psychol. *6*, 1805. https://doi.org/10.3389/fpsyg.2015.01805.
10. Smith, D.V., Clithero, J.A., Boltuck, S.E., and Huettel, S.A. (2014). Functional connectivity with ventromedial prefrontal cortex reflects subjective value for social rewards. Soc. Cognit. Affect Neurosci. *9*, 2017–2025. https://doi.org/10.1093/scan/nsu005.

11. Dai, B., Sun, F., Tong, X., Ding, Y., Kuang, A., Osakada, T., Li, Y., and Lin, D. (2022). Responses and functions of dopamine in nucleus accumbens core during social behaviors. Cell Rep. *40*, 111246. https://doi.org/10.1016/j.celrep.2022.111246.

12. Dölen, G., Darvishzadeh, A., Huang, K.W., and Malenka, R.C. (2013). Social reward requires coordinated activity of nucleus accumbens oxytocin and serotonin. Nature *501*, 179–184. https://doi.org/10.1038/nature12518.

13. Park, G., Ryu, C., Kim, S., Jeong, S.J., Koo, J.W., Lee, Y.S., and Kim, S.J. (2021). Social isolation impairs the prefrontal-nucleus accumbens circuit subserving social recognition in mice. Cell Rep. *35*, 109104. https://doi.org/10.1016/j.celrep.2021.109104.

14. Sheehan, T., and Numan, M. (2000). The Septal Region and Social Behavior. In The Behavioral Neuroscience of the Septal Region, R. Numan, ed. (Springer), pp. 175–209. https://doi.org/10.1007/978-1-4612-1302-4_8.

15. Goodson, J.L., Eibach, R., Dukes, A., Friedman, M., Sakata, J., Thompson, R., and Adkins-Regan, E. (1997). Neurobiology of Avian Social Organization Effects of Lateral Septum Lesions in a Territorial Songbird, the Field Sparrow (Spizella pusilla), and a Colonial Songbird, the Zebra Finch (Taeniopygia guttata). Ann. N. Y. Acad. Sci. *807*, 518–521. https://doi.org/10.1111/j.1749-6632.1997.tb51956.x.

16. Noonan, M.P., Sallet, J., Mars, R.B., Neubert, F.X., O'Reilly, J.X., Andersson, J.L., Mitchell, A.S., Bell, A.H., Miller, K.L., and Rushworth, M.F.S. (2014). A Neural Circuit Covarying with Social Hierarchy in Macaques. PLoS Biol. *12*, e1001940. https://doi.org/10.1371/journal.pbio.1001940.

17. Clemens, A.M., Wang, H., and Brecht, M. (2020). The lateral septum mediates kinship behavior in the rat. Nat. Commun. *11*, 3161. https://doi.org/10.1038/s41467-020-16489-x.

18. Diaconescu, A.O., Mathys, C., Weber, L.A.E., Kasper, L., Mauer, J., and Stephan, K.E. (2017). Hierarchical prediction errors in midbrain and septum during social learning. Soc. Cognit. Affect Neurosci. *12*, 618–634. https://doi.org/10.1093/scan/nsw171.

19. Jung, F., and Carlén, M. (2021). Chapter Twelve - Neuronal oscillations and the mouse prefrontal cortex. In *International Review of Neurobiology*. Vol 158. What does Medial Frontal Cortex Signal During Behavior? Insights from Behavioral Neurophysiology, A.T. Brockett, L.M. Amarante, M. Laubach, and M.R. Roesch, eds. (Academic Press), pp. 337–372. https://doi.org/10.1016/bs.irn.2020.11.005.

20. Jacobs, J. (2014). Hippocampal theta oscillations are slower in humans than in rodents: implications for models of spatial navigation and memory. Philos. Trans. R. Soc. Lond. B Biol. Sci. *369*, 20130304. https://doi.org/10.1098/rstb.2013.0304.

21. Herweg, N.A., Solomon, E.A., and Kahana, M.J. (2020). Theta Oscillations in Human Memory. Trends Cognit. Sci. *24*, 208–227. https://doi.org/10.1016/j.tics.2019.12.006.

22. Colgin, L.L. (2011). Oscillations and hippocampal–prefrontal synchrony. Curr. Opin. Neurobiol. *21*, 467–474. https://doi.org/10.1016/j.conb.2011.04.006.

23. Harris, A.Z., and Gordon, J.A. (2015). Long-Range Neural Synchrony in Behavior. Annu. Rev. Neurosci. *38*, 171–194. https://doi.org/10.1146/annurev-neuro-071714-034111.

24. Welle, C.G., and Contreras, D. (2016). Sensory-driven and spontaneous gamma oscillations engage distinct cortical circuitry. J. Neurophysiol. *115*, 1821–1835. https://doi.org/10.1152/jn.00137.2015.

25. Jensen, O., Kaiser, J., and Lachaux, J.P. (2007). Human gamma-frequency oscillations associated with attention and memory. Trends Neurosci. *30*, 317–324. https://doi.org/10.1016/j.tins.2007.05.001.

26. Magazzini, L., and Singh, K.D. (2018). Spatial attention modulates visual gamma oscillations across the human ventral stream. Neuroimage *166*, 219–229. https://doi.org/10.1016/j.neuroimage.2017.10.069.

27. Buzsáki, G., and Wang, X.J. (2012). Mechanisms of Gamma Oscillations. Annu. Rev. Neurosci. *35*, 203–225. https://doi.org/10.1146/annurev-neuro-062111-150444.

28. Headley, D.B., and Paré, D. (2013). In sync: gamma oscillations and emotional memory. Front. Behav. Neurosci. *7*, 170. https://doi.org/10.3389/fnbeh.2013.00170.

29. Mohapatra, A.N., Peles, D., Netser, S., and Wagner, S. (2024). Synchronized LFP rhythmicity in the social brain reflects the context of social encounters. Commun. Biol. *7*, 2. https://doi.org/10.1038/s42003-023-05728-8.

30. Tendler, A., and Wagner, S. (2015). Different types of theta rhythmicity are induced by social and fearful stimuli in a network associated with social memory. eLife *4*, e03614. https://doi.org/10.7554/eLife.03614.

31. Mohapatra, A.N., Netser, S., and Wagner, S. (2022). Modular Electrode Array for Multi-site Extracellular Recordings from Brains of Freely Moving Rodents. Curr. Protoc. *2*, e399. https://doi.org/10.1002/cpz1.399.

32. Netser, S., Haskal, S., Magalnik, H., Bizer, A., and Wagner, S. (2019). A System for Tracking the Dynamics of Social Preference Behavior in Small Rodents. J. Vis. Exp. *153*, 60336. https://doi.org/10.3791/60336-v.

33. Mathis, A., Mamidanna, P., Cury, K.M., Abe, T., Murthy, V.N., Mathis, M.W., and Bethge, M. (2018). DeepLabCut: markerless pose estimation of user-defined body parts with deep learning. Nat. Neurosci. *21*, 1281–1289. https://doi.org/10.1038/s41593-018-0209-y.

34. Goodwin, N.L., Choong, J.J., Hwang, S., Pitts, K., Bloom, L., Islam, A., Zhang, Y.Y., Szelenyi, E.R., Tong, X., Newman, E.L., et al. (2024). Simple Behavioral Analysis (SimBA) as a platform for explainable machine learning in behavioral neuroscience. Nat. Neurosci. *27*, 1411–1424. https://doi.org/10.1038/s41593-024-01649-9.

35. John, S.R., Dagash, W., Mohapatra, A.N., Netser, S., and Wagner, S. (2022). Distinct Dynamics of Theta and Gamma Rhythmicity during Social Interaction Suggest Differential Mode of Action in the Medial Amygdala of Sprague Dawley Rats and C57BL/6J Mice. Neuroscience *493*, 69–80. https://doi.org/10.1016/j.neuroscience.2022.04.020.

36. Mohapatra, A.N., Jabarin, R., Ray, N., Netser, S., and Wagner, S. (2025). Impaired emotion recognition in Cntnap2-deficient mice is associated with hyper-synchronous prefrontal cortex neuronal activity. Mol. Psychiatr. *30*, 1440–1452. https://doi.org/10.1038/s41380-024-02754-8.

37. Bressler, S.L., and Menon, V. (2010). Large-scale brain networks in cognition: emerging methods and principles. Trends Cognit. Sci. *14*, 277–290. https://doi.org/10.1016/j.tics.2010.04.004.

38. Fries, P. (2015). Rhythms for Cognition: Communication through Coherence. Neuron *88*, 220–235. https://doi.org/10.1016/j.neuron.2015.09.034.

39. Jabarin, R., Mohapatra, A.N., Ray, N., Netser, S., and Wagner, S. (2025). Distinct prelimbic cortex neuronal responses to emotional states of others drive emotion recognition in adult mice. Curr. Biol. *35*, 994–1011.e8. https://doi.org/10.1016/j.cub.2025.01.014.

40. Barnett, S.A. (1958). An Analysis of Social Behaviour in Wild Rats. Proc. Zool. Soc. Lond. *130*, 107–152. https://doi.org/10.1111/j.1096-3642.1958.tb00565.x.

41. Cui, Q., Li, Q., Geng, H., Chen, L., Ip, N.Y., Ke, Y., and Yung, W.H. (2018). Dopamine receptors mediate strategy abandoning via modulation of a specific prelimbic cortex–nucleus accumbens pathway in mice. Proc. Natl. Acad. Sci. USA *115*, E4890–E4899. https://doi.org/10.1073/pnas.1717106115.

42. Kietzman, H.W., Trinoskey-Rice, G., Blumenthal, S.A., Guo, J.D., and Gourley, S.L. (2022). Social incentivization of instrumental choice in mice requires amygdala-prelimbic cortex-nucleus accumbens connectivity. Nat. Commun. *13*, 4768. https://doi.org/10.1038/s41467-022-32388-9.

43. van Aerde, K.I., Heistek, T.S., and Mansvelder, H.D. (2008). Prelimbic and Infralimbic Prefrontal Cortex Interact during Fast Network Oscillations. PLoS One *3*, e2725. https://doi.org/10.1371/journal.pone.0002725.

44. Mukherjee, A., and Caroni, P. (2018). Infralimbic cortex is required for learning alternatives to prelimbic promoted associations through reciprocal connectivity. Nat. Commun. *9*, 2727. https://doi.org/10.1038/s41467-018-05318-x.

45. Einevoll, G.T., Kayser, C., Logothetis, N.K., and Panzeri, S. (2013). Modelling and analysis of local field potentials for studying the function of cortical circuits. Nat. Rev. Neurosci. *14*, 770–785. https://doi.org/10.1038/nrn3599.

46. Phalip, A., Netser, S., and Wagner, S. (2024). Understanding the neurobiology of social behavior through exploring brain-wide dynamics of neural activity. Neurosci. Biobehav. Rev. *165*, 105856. https://doi.org/10.1016/j.neubiorev.2024.105856.

47. Cohen, L., Mohapatra, A.N., Netser, S., Wagner, S., and Stark, E. (2025). Social remapping of spatial coding along the dorsoventral axis of the mouse prefrontal cortex. Cell Rep. *44*, 116319. https://doi.org/10.1016/j.celrep.2025.116319.

48. Popik, P., Cyrano, E., Piotrowska, D., Holuj, M., Golebiowska, J., Malikowska-Racia, N., Potasiewicz, A., and Nikiforuk, A. (2023). Effects of ketamine on rat social behavior as analyzed by DeepLabCut and SimBA deep learning algorithms. Front. Pharmacol. *14*, 1329434. https://doi.org/10.3389/fphar.2023.1329424.

STAR★METHODS

KEY RESOURCES TABLE

REAGENT or RESOURCE	SOURCE	IDENTIFIER
Bacterial and virus strains		
ssAAV-1/2-mCaMK2a-GCaMP6f-WPRE-SV40p(A)	Zurich VVF, Switzerland	183
Chemicals, peptides, and recombinant proteins		
Ketamine (Ketaset)	Zoetis Inc. Spain	507340
Domitor	ORION CORPORATION ORION PHARMA, FINLAND	082-58-92306-00
meloxicam (LOXICOM)	NORBROOK LABORATORIES LTD, IRELAND	150-41-33607-00
Isoflurane	PIRAMAL CRITICAL CARE INC., USA	105-52-28997-00
Ophthalmic ointment (Duratears)	ALCON COUVREUR N.V., BELGIUM	109-33-24050-00
dental cement	UNIFAST, GC America	GC-5150316
antisedan	ORION CORPORATION ORION PHARMA, FINLAND	141-85-92305-01
baytril	ELANCO ANIMAL HEALTH GMBH	082-15-91819-00
paraformaldehyde (PFA)	Sigma	818708
DAPI (fluoroshield with DAPI)	Abcam	ab104139
Deposited data		
Dataset	Mendeley data	https://doi.org/10.17632/zpb4vhkyvg.1
Experimental models: Organisms/strains		
C57BL/6 J mice	Envigo RMS, Israel	N/A
CD-1 mice	Envigo RMS, Israel	N/A
SD rats	Envigo RMS, Israel	N/A
Software and algorithms		
Graphpad	Prism	v10.1.2
FlyCapture2	FLIR	FlyCap2Viewer_2.13.3.61_×64.exe
TrackRodent	https://github.com/shainetser/TrackRodent	N/A
DeepPhenotyping	https://doi.org/10.5281/zenodo.10708903	N/A
Flea3 USB3	Flir	FL3-U3-13E4M-C
Other		
RHD2000 evaluation system	Intan Technologies	C3100
Optic fibers (200 μm, NA 0.66, 4 mm long, zirconia ferrule, flat-fiber tip)	Doric lenses	200/250–0.66 T
power meter	Thorlabs	PM100D
Ti2 fluorescent microscope	Nikon	N/A
VT1200s sliding vibratome	Leica	N/A
SomnoSuite	Kent Scientific Corporation	N/A
stereotaxic apparatus	Kopf	Model 963
Optical patch cord with a fiber-optic rotary joint	Tucker-Davis Technologies	FRJ_1 × 1_PT_200/230/LWMJ-0.57_1 m_FCM_0.15 m_FCM
disposable BLAUBRAND micropipettes (intraMark, 5 μL)	BRAND	708707
Four ports Fluorescence MiniCube	Tucker-Davis Technologies	iIFMC4-G3_IE(400–410)_E(460–490)_F(500–550)_S

EXPERIMENTAL MODEL AND STUDY PARTICIPANT DETAILS

Adult male C57BL/6 J and CD1 mice (12–14 weeks old) were purchased from Envigo (Rehovot, Israel). Adult Sprague-Dawley (SD) rats (12–16 weeks old) were bred in the animal facility of the University of Haifa. Stimulus animals were sex-matched conspecifics bred in the animal facility at University of Haifa. All the animals were reared in the animal facility of the University of Haifa under veterinary supervision in a reversed 12 h light/12 h dark cycle (lights on at 7 p.m.) with *ad libitum* access to food (standard chow diet, Envigo RMS, Israel) and water. All experiments were accomplished according to the National Institutes of Health guide for the care and use of laboratory animals and approved by the Institutional Animal Care and Use Committee of the University of Haifa (C57: #1077U, CD1: license #616/19, SD: #1664U).

METHOD DETAILS

Experimental setup

As previously described,[32] a Plexiglas "arena" (black, 50 × 50 × 40 cm for SD rats and 30 × 22 × 35 cm for CD1 mice; white, 30 × 22 × 35 cm for C57 mice) was located within an acoustic cupboard. The cupboard was equipped with a monochromatic camera (Flea3 USB3, Point Gray), furnished with a wide-angle lens to provide a clear view and recording (30 frames/s) of the subject's behavior using a commercial software (FlyCapture2, Point Gray). Two Plexiglas triangular stimulus "chambers" (20.5 cm isosceles, 40 cm stature for rats; 12 cm × 12 cm × 35 cm for mice), with a metal mesh to cover the bottom and allow direct interaction with the social stimulus, were set in two randomly chosen opposite corners of the arena for the SP task (See Figure 1A for details). The recordings took place under red light to ensure that there is no effect of the color of the arena or chambers on the behavior of the animals.

Behavioral paradigms

Social preference task (SP)

As previously described,[29,32,35] subject animals were briefly anesthetized with isoflurane to connect them with the headstage (RHD 32 ch, #C3314, Intan Technologies) through a custom-made Omnetics to Mill-Max adaptor (Mill-Max model 852-10- 100-10-001000). Then, the subject animals were placed in an empty arena for 15 min, followed by habituation with empty triangular chambers located in the arena for 15 min. Each recording session was 10 min long, starting with a 5-min baseline stage, which followed by 5-min encounter stage with novel object (a Lego toy) and social (sex-matched conspecific) stimuli placed inside the chambers (Figure 1A). Notably, in this task social interactions were restricted by the stimulus chamber's metal mesh separating between them.

Free interaction (FI)

Subject animals were habituated to the empty arena for 15 min. Then, a recording session of 10 min was initiated with a 5-min baseline stage in the empty arena, followed by a 5-min encounter stage with a sex-matched conspecific introduced to the arena (Figure 1B).

Most animals performed both SP and FI tasks, with 1–3 sessions of each task recorded from each animal (number of animals, C57, n = 11, CD1, n = 14, SD rats, n = 13, See Table S3 for details). The order of tasks was randomized.

Stereotactic surgery for implantation of electrode array and optic fiber

Electrode array: Electrode Array (EAr) were fabricated as previously described.[31] Animals were anesthetized by the intraperitoneal administration of ketamine and Domitor (90 mg/kg body weight of the animal and 5.5 mg/kg body weight of the animal, respectively for rats; 130 mg/kg body weight of the animal and 10 mg/kg body weight of the animal for mice). The depth of anesthesia was confirmed by toe pinch reflexes. The body temperature of the animals was kept constant at approximately 37°C using a custom-made temperature controller connected to a temperature probe and a heating pad placed under the animal. Anesthetized animals were fixed in a stereotaxic apparatus (Stoelting Inst. For rats and Kopf Inst. For mice), keeping the head flat using ear bars. The eyes were covered by duratears (Alcon couvreur N.V., Belgium) to prevent drying of the cornea. To maintain the anesthetized state, isoflurane was constantly supplied to the nose (Somnoflow low-flow electronic Anesthesia system, Kent scientific). Skin was removed carefully using a scalpel and scissors. To clean the blood, cold 0.01 M PBS was applied to the incised portion. Craniotomy was performed, and the skull was gently removed using a sharp bent needle, followed by two stainless steel screws fixed from both sides of the craniotomy. PRL, IL, AcbS, AcbC, and LS were targeted with the EAr (see Table S2 for coordinates). The electrode aimed to Paraventricular Nucleus of Hypothalamus (PVN) (AP = −1 mm, ML = −0.3, DV = −4.7) in mice and AcbS (A/P = +1 mm, L/M = ±2 mm, D/V = −7.6 mm) in rats was used as a reference for the coordinates of the EAr. The EAr was dipped in DiI (1,1′-Dioctadecyl3,3,3′,3′-tetramethylindocarbocyanine perchlorate; 42364, SigmaAldrich) before implantation. Lastly, using toothpicks, a mixture of histoacryl and dental cement was applied to the surrounding skull to fix the implant to the skull.

Optic fiber: The surgery procedure until brain perturbation was as described above for electrode arrays. After exposing the skull, the region of the mPFC was marked, and a hole (unilateral, right hemisphere) was drilled for viral injection and optic fiber implantation. Additional holes were drilled for supporting screws. Viral injection was performed as previously described in detail (https://starprotocols.cell.com/protocols/1283) using a glass capillary filled with the virus (ssAAV-1/2-mCaMK2a-GCaMP6f-WPRE-SV40p(A), VVF, Zurich, Switzerland, Physical titer: 6.2 × 10^{12} vp/mL) was slowly lowered into the PRL (AP,+1.9 mm; ML,

−0.35 mm; DV, +2.0 mm for mice and AP,+3.0 mm; ML, −0.6 mm; DV, +4.0 mm for rats) and left in place for 5 min prior to injection and 10 min following injection to prevent retraction of the virus. A total of 300 nL of the virus was delivered by manual application using a 50 mL syringe connected to the glass capillary for applying air pressure (BRAND, disposable BLAUBRAND micropipettes, intra-Mark, 5 mL). Following viral injection, an optic fiber (Doric lenses, 200 mm, NA 0.66, 3 mm long for mice and 5 mm for rat, zirconia ferrule, flat-fiber tip) was inserted into the PrL with the same coordinates as the viral injection and placed 200 μm above the injection depth. Following implantation, screws and optic fiber were fixed to the skull plate using dental cement (UNIFAST, GC America).

Recovery: Antisedan (2 mg/kg body weight for the rat, 0.1 mL/10 g bodyweight for mice) was given subcutaneously to wake the animals from the anesthesia. Meloxicam (0.01 mg/g for both rats and mice) and baytril (5 mg/kg body weight for rats and 0.03 mL/10 g for mice) were administered to relieve pain and prevent infections for three days following surgery. Experiments were performed after at least 7 days of recovery. The targeted brain areas for each animal are summarized in Table S2.

Data acquisition

Electrophysiology: Electrophysiological data was recorded via the RHD2000 evaluation system using an ultra-thin SPI interface cable and a RHD2132 amplifier board (Intan Technologies). Recorded signals (sampled at 20 kHz) were collected simultaneously from all targeted brain regions and synchronized with the video recording by a start signal sent through a custom-made triggering device and TTL signals from the camera to the recording system. Specifically, the signals in theta (4–12 Hz) and gamma (30–80 Hz) bands were extracted using a bandpass filter due to their significant role in social behavior.[46]

Fiber photometry: The optic fiber of the implanted animal was connected to the optical patch cords via a sleeve connector (Doric), with brief (5–10 s) isoflurane anesthesia used only in mice, as previously described.[47] The wired animal was then allowed to habituate in the arena for 15 min before the recording session. Calcium signals were recorded using the RZ10× system of Tucker Davis Technologies and an optical path by Doric, which includes 600 μm mono-fiber optic patch cords connected to a four ports Fluorescence MiniCube (FMC4_IE(400–410)_E(460–490) _F(500–550)_S) and a 200 μm optical patch cord with a fiber-optic rotary joint (FRJ_131_PT_200/230/LWMJ-0.57_1 m_FCM_ 0.15 m_FCM) connected to the recorded animal. A camera (Flea3 USB3, FLIR) was placed on top of the arena and connected to the digital port of the RZ103 system and configured to deliver strobes for every frame acquired at a frame rate of 30 frames/s. These were later used to synchronize the video frames with the calcium signal. TDT Synapse software was used for recording the GCaMP6f signal channel (excitation 465 nm, modulated at 330 Hz), the isosbestic control channel (405 nm, modulated at 210 Hz) and the digital channel receiving the camera strobes, using a sampling rate of 1017.3 Hz.

Histological analysis for electrode registration

After finishing all experiments, animals were anesthetized using an overdose of isofluran and then perfused with 0.01 M phosphate buffer saline (PBS), followed by fixation in 4% paraformaldehyde (PFA) solution. After implant removal, brains were harvested and placed in PFA (4%) for three to four days, followed by sectioning of 50-μm slices in the horizontal axis for electrode tracing or coronal axis for optic fiber tracing, using a vibratome (VT1000s, Leica). Sections were stained with DAPI and examined under a wide-field fluorescence microscope (Nikon Ti-eclipse) for verifying the placement of the electrode marks, i.e., DiI fluorescence (Figure 2B).

QUANTIFICATION AND STATISTICAL ANALYSIS

Video tracking and behavioral analysis

SP sessions: Video clips were analyzed using TrackRodent as previously described.[32] The videos of C57 mice were analyzed using the BlackMouseWiredBodyBased4_11_15 algorithm, CD1 mice using the WhiteMouseWiredBodyBased3_7_19 algorithm, and SD rats using the WhiteRatsWiredHeadDirectBased13_1_2019 algorithm. In all cases, the chambers were marked using the software such that when the animal is closer than 2 cm to the chamber, it is considered as an interaction. An interaction of longer than 2 s with the chamber was defined as an investigation bout, with interruptions of <0.5 s being ignored.

The relative discrimination index (RDI) was calculated as follows:

$$RDI = \frac{Social\ investigation\ time - Object\ investigation\ time}{Total\ investigation\ time}$$

$$Total\ investigation\ time = Social\ investigation\ time + Object\ investigation\ time$$

FI sessions: We used DeepLabCut (version 2.3.8, [33]) for multi-animal body part tracking. The two freely interacting animals were marked as ''subject'' or ''stimulus''. We labeled eight body parts, namely left and right ears, nose, neck, trunk, left and right lateral body, and tail base (Figure 2A). We annotated 600 frames from C57 mice extracted from three videos, 3200 frames for CD1 mice from 16 videos and 800 frames for SD rats extracted from four videos. A dlcrnetms5-based neural network was employed with default parameters for 2*106 training iterations. We used the outlier corrections step to improve the model. The test errors were 5.43, 6.33, and 5.5 pixels and training error was 3.32, 3.73, and 4.42 pixels respectively for C57 mice, CD1 mice, and SD rats (SupFig1 B-D). These networks were then used to analyze the test videos from similar experimental settings.

Next, we employed SimBA[34] to train models for supervised behavior classification of the subject animals. Since the body part "Nose" had maximum error and was undetected by DeepLabCut in many frames, we prepared a custom python script for feature extraction such that the detection of "Nose" is not crucial. This script was materialised with the help of the video analysis pipeline by Popik et al.[48] SimBA version 1.55.6 was used for feature extraction using a custom python script (https://github.com/98rishika/Mouse-rat_analysis.git). The independent random forest classifier models were trained for all the strains in version 2.9.6. Following behaviors were labeled.

- *Sniff_Ano* – sniffing of the anogenital area of the stimulus by the subject animal
- *Sniff_body* – sniffing of the body (excluding anogenital and head areas) of the stimulus animal by the subject
- *NosetoNose* – Investigation of head areas of each other by both animals
- *Move* – Non-social movements of subject animal
- *Sit_idle* – Non-social resting of the subject animal

The performance of the model was determined using classification report metrics. All the models used for analyses achieved the F1 score of more than 0.80. 13 out of 34 videos from CD1 mice were removed from the analysis due to poor body parts detection in DeepLabCut. In 5 sessions, CD1 mice displayed aggressive behaviors such as fighting and tail rattling. Therefore, for CD1 mice, we also trained SimBA to detect the *Fight* and *Tail_rattle* bouts. However, due to the poor classification of these behaviors by the model (F1 score for fight – 73% and for Tail_rattle – 68.9%), we did not include the results here.

Electrophysiological analysis

All electrophysiology signals were analyzed using a custom-made MATLAB program. First, the signals were down-sampled to 5 kHz and low-pass filtered up to 300 Hz using a Butterworth filter. The power over time for the different frequencies were constructed by the *spectrogram* function in MATLAB, using a 2 s long discrete prolate spheroidal sequences (DPSS) window with 50% overlap, at 0.5 Hz increments and 0.5 s time bins. The power for each frequency band (Theta: 4–12 Hz and Gamma: 30–80 Hz) was averaged. For the change in power during the encounter stage, we subtracted the mean power averaged across the entire 5 min of baseline stage from the one calculated for the encounter stage.

Fiber photometry analysis

Calcium signals were analyzed using DeepPhenotyping as previously described.[39] We first fitted the 405 nm channel onto the 465 nm channel to de-trend signal bleaching and any movement artifacts, according to the manufacturer's protocol (https://github.com/tjd2002/tjd-sharedcode/blob/master/matlab/photometry/FP_normalize.m). Next, we obtained the detrended signal amplitude values from DeepPhenotyping and normalized these values for the whole session using Z score, with the baseline stage used as a baseline for Z-scoring the signal. For analysing the recorded signal around specific investigation bout events, the de-trended signal was aligned to the video recording using the timestamps recorded by the digital port of the RZ10$\times$ system. We then aligned the de-trended signal to each behavioral event (all/long bouts) and normalized it using the Z score (0.5 s bins), with the pre-event time window of -4 s to -1 s serving as a baseline. This time window was selected as it allows a good separation of the current investigation bout from the previous one, typically occurring >4s earlier, while also allowing to detect signal deviations from baseline which may take place within 1 s before the detected contact of the subject with the stimulus chamber[39] As for calculating the population average signal amplitude over time, we first calculated the AUC for each session in time bins of 5 s (using the original detrended signal which is samples at 1017.3 Hz) and then averaged the signals across all sessions.

Statistical analysis

Statistical tests were performed using GraphPad Prism version 9.0.0 for Windows, GraphPad Software, San Diego, California USA, www.graphpad.com (see Table S1 for the details of all statistical analyses). Normality of the data was tested using Shapiro-Wilk or Anderson-Darling (A2) test. One-way ANOVA or Kruskal-Wallis tests were performed to compare multiple groups like different strains and stages of the social interaction. Upon finding a main effect or interaction in the tests above, Sidak's or Dunn's post-hoc multiple comparison corrections were applied. two-way ANOVA was used to compare multiple groups and parameters.

PCA

A comprehensive set of 22 electrophysiological features was extracted from local field potential (LFP) recordings obtained from five brain regions: IL, PRL, AcbC, AcbS, and LS. The feature set comprised.

- Theta power (4–12 Hz) in each of the 5 brain regions
- Gamma power (30–80 Hz) in each of the 5 brain regions
- Theta coherence between all possible brain region pairs where sufficient recordings were available ($n \geq 5$ from all strains)
- Gamma coherence between the same brain region pairs

PCA was performed separately for SP and FI sessions to cluster strains and experimental stages (baseline and interaction) according to their electrophysiological profiles. The analysis combined data from all three strains and both experimental stages (baseline and encounter) within each task type.

All 22 electrophysiological features were standardized using StandardScalar function from sklearn to ensure equal weighting across different measurement scales and units. Data from all strains (C57, CD1, SD) and both experimental stages (baseline, encounter) were combined into a single dataset for each task type (SP and FI separately). PCA was applied to reduce the 22-dimensional feature space to the principal components that captured the maximum variance in the electrophysiological data. The top two principal component scores were used to visualize clustering patterns and calculate distances between different strain-stage combinations.

Euclidean distances between clusters were calculated to quantify the degree of electrophysiological differentiation between experimental conditions.

Random forest classifier

The classification analysis utilized the same 22 electrophysiological features employed in the PCA analysis. Given the limited sample sizes inherent in electrophysiological recordings from laboratory animals (C57: $n = 22$ for SP, $n = 23$ for FI; CD1: $n = 33$ for SP, $n = 34$ for FI; SD: $n = 20$ for SP, $n = 12$ for FI), we implemented a robust multiple imputation strategy to address potential missing data and enhance the reliability of our classification results. 100 imputed datasets were generated for each experimental condition. The missing values were imputed using KNN imputation based on the relationships between electrophysiological features. To identify which electrophysiological features most contributed to strain classification, we calculated feature importance scores using RandomForestClassifier.feature_importances_ function for each of the 1,000 classification experiments. Shuffled controls were generated by randomly permuting strain labels while maintaining the electrophysiological feature structure. Performance was compared against shuffled labels classification (Mann-Whitney U test, $p < 0.0001$ for all models, Figure S4). Statistical comparisons between the feature importance obtained from true and the shuffled labeled data were performed using effect size (Cohen's d). The value of 0.8 was set as threshold to determine meaningful difference (Table S1). Codes are available at https://github.com/98rishika/Mouse-rat_analysis.git.